



RESEARCH ARTICLE

10.1002/2017EA000329

Key Points:

- Solar radiation pressure spins-up defunct TOPEX/Poseidon spacecraft
- An 11 year spin trend is measured by optical methods
- A complete satellite attitude model is developed for perturbation analysis

Correspondence to:

D. Kucharski,
danielkucharski@serc.org.au

Citation:

Kucharski, D., Kirchner, G., Bennett, J. C., Lachut, M., Sońnica, K., Koshkin, N., ... Suchodolski, T. (2017). Photon pressure force on space debris TOPEX/Poseidon measured by satellite laser ranging. *Earth and Space Science*, 4, 661–668. <https://doi.org/10.1002/2017EA000329>





Received 8 AUG 2017

Accepted 24 SEP 2017

Accepted article online 4 OCT 2017

Published online 30 OCT 2017

Photon Pressure Force on Space Debris TOPEX/Poseidon Measured by Satellite Laser Ranging

D. Kucharski^{1,2} , G. Kirchner², J. C. Bennett¹, M. Lachut¹, K. Sońnica³ , N. Koshkin⁴, L. Shakun⁴, F. Koidl², M. Steindorfer², P. Wang², C. Fan⁵, X. Han⁵, L. Grunwaldt⁶, M. Wilkinson⁷, J. Rodríguez⁷, G. Bianco⁸, F. Vespe⁸, M. Catalán⁹, K. Salmins¹⁰ , J. R. del Pino¹⁰ , H.-C. Lim¹¹, E. Park¹¹, C. Moore¹², P. Lejba¹³, and T. Suchodolski¹³

¹Space Environment Research Centre, Canberra, ACT, Australia, ²Space Research Institute, Austrian Academy of Sciences, Graz, Austria, ³Institute of Geodesy and Geoinformatics, Wrocław University of Environmental and Life Sciences, Wrocław, Poland, ⁴Astronomical Observatory of Odessa Mechnikov University, Odessa, Ukraine, ⁵Changchun Observatory, NAO, Chinese Academy of Sciences, Changchun, China, ⁶Helmholtz Center Potsdam, German Research Centre for Geosciences GFZ, Potsdam, Germany, ⁷Natural Environment Research Council, Space Geodesy Facility, Herstonceux, UK, ⁸Agenzia Spaziale Italiana, Centro di Geodesia Spaziale “G. Colombo”, Matera, Italy, ⁹Royal Observatory of the Spanish Navy, San Fernando, Spain, ¹⁰Institute of Astronomy, University of Latvia, Riga, Latvia, ¹¹Space Science Division, Korea Astronomy and Space Science Institute, Daejeon, South Korea, ¹²EOS Space Systems Pty. Ltd., Canberra, ACT, Australia, ¹³Space Research Centre, Polish Academy of Sciences, Astrogeodynamic Observatory, Borowiec, Poland

Abstract The (TOPography EXperiment) TOPEX/Poseidon (T/P) altimetry mission operated for 13 years before the satellite was decommissioned in January 2006, becoming a large space debris object at an altitude of 1,340 km. Since the end of the mission, the interaction of T/P with the space environment has driven the satellite’s spin dynamics. Satellite laser ranging (SLR) measurements collected from June 2014 to October 2016 allow for the satellite spin axis orientation to be determined with an accuracy of 1.7°. The spin axis coincides with the platform yaw axis (formerly pointing in the nadir direction) about which the body rotates in a counterclockwise direction. The combined photometric and SLR data collected over the 11 year time span indicates that T/P has continuously gained rotational energy at an average rate of 2.87 J/d and spins with a period of 10.73 s as of 19 October 2016. The satellite attitude model shows a variation of the cross-sectional area in the Sun direction between 8.2 m² and 34 m². The direct solar radiation pressure is the main factor responsible for the spin-up of the body, and the exerted photon force varies from 65 μN to 228 μN around the mean value of 138.6 μN. Including realistic surface force modeling in orbit propagation algorithms will improve the prediction accuracy, giving better conjunction warnings for scenarios like the recent close approach reported by the ILRS Space Debris Study Group—an approximate 400 m flyby between T/P and Jason-2 on 20 June 2017.

1. Introduction

1.1. TOPEX/Poseidon Mission

Ocean TOPography EXperiment TOPEX/Poseidon (T/P, NORAD 22076) was a joint project between the National Aeronautics and Space Administration (NASA) and the French Space Agency, Centre National d’Etudes Spatiales (CNES) (Fu et al., 1994) designed to explore ocean circulation and its interaction with the atmosphere. The satellite was launched on 10 August 1992 into a circular orbit with a perigee of 1,340 km and an inclination of 66°. The spacecraft has a mass of 2,400 kg and was nadir stabilized during the mission – Figure 1 (Tapley et al., 1994). The onboard altimeters measured the distance to the instantaneous sea surface with a precision of about 2 cm and helped to better understand global climate change and weather phenomena such as El Niño. Three independent techniques (SLR, DORIS, and GPS) were used to determine the satellite altitude for the altimeter calibration. The retroreflector array (RRA) used for laser ranging to the satellite is constructed as an angled ring (1.5 m diameter) fitted around the nadir-pointed altimeter antenna—Figure 1 (Schwartz, 1990). The RRA is made up of 192 corner cube reflectors arranged in two rows with the entrance face normals off-pointed from the nadir axis by 40°.

On 9 October 2005, the satellite’s pitch momentum wheel stopped functioning, which kept the spacecraft in its proper orbital orientation. On 5 January 2006 T/P was decommissioned (Paredes et al., 2008) concluding a 13 year mission that transformed the understanding of ocean dynamics.

©2017. The Authors.

This is an open access article under the terms of the Creative Commons Attribution-NonCommercial-NoDerivs License, which permits use and distribution in any medium, provided the original work is properly cited, the use is non-commercial and no modifications or adaptations are made.

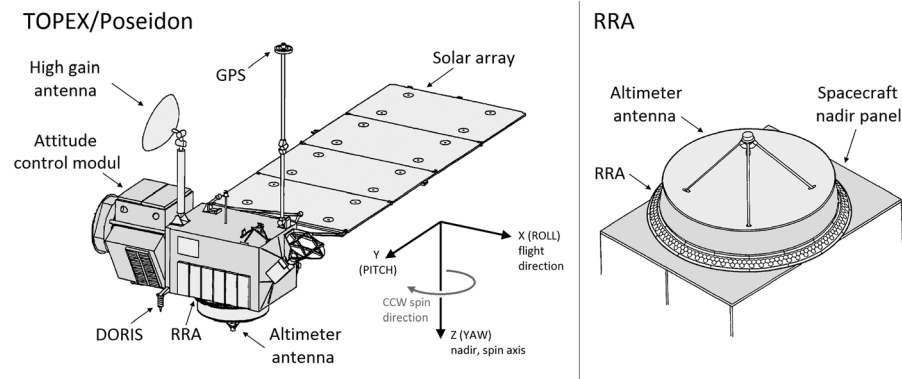


Figure 1. TOPEX/Poseidon satellite. (left) The spacecraft’s body. (right) The nadir panel with retroreflector array RRA and altimeter antenna.

1.2. Laser Range Measurements and Light Curves of Defunct TOPEX/Poseidon

During the active phase of the mission, T/P was nadir stabilized and the solar panel was kept oriented toward the Sun. After becoming a passive space debris object, T/P started gaining rotational energy and was frequently observed by satellite laser ranging (SLR) and photometric systems.

SLR measures distances between the ground station and satellites equipped with corner cube reflectors (CCRs). During a satellite pass over an SLR station the transmitted laser pulses are reflected by the CCRs back to the receiver telescope of the tracking system. After the pass a simple scheme that fits the predicted orbit to the observations is used, and the range residuals are calculated as a difference between measured and predicted range values. In the course of this process we use the orbit fit method developed by the Herstmonceux Space Geodesy Facility, which estimates the time bias and range bias coefficients to provide a smooth representation of the reference orbit. The laser ranging data is used for the accurate orbit predictions and conjunction analysis (Bennett et al., 2013; Wirnsberger et al., 2015). The SLR tracking of defunct T/P was initiated in 2014 by the Graz SLR station (Austria) (Kirchner et al., 2013) and subsequently in 2015 by the Space Debris Study Group of the International Laser Ranging Service (ILRS) (Pearlman et al., 2002). The collected laser ranging data is available on the Graz Space Debris Server (ftp://sddis.oeaw.ac.at).

The Odessa photometric system has acquired light curves of T/P since the end of the mission (Shakun et al., 2016). The system measures the intensity of sunlight reflected from the surface of the tracked satellites toward the ground telescope. The intensity of the detected light depends mainly on the following: (1) the angular configuration between the direction to the Sun, the ground system, and the normal vectors to the satellite surface elements, (2) the optical properties of the satellite body, and (3) the slant range to the satellite and the atmospheric conditions during the pass. The measured brightness is corrected for the atmospheric absorption and expressed as the standard magnitude at the distance of 1,000 km (Koshkin et al., 2016). The brightness modulation of the sunlit satellite allows for the spin parameters determination during the nighttime periods only.

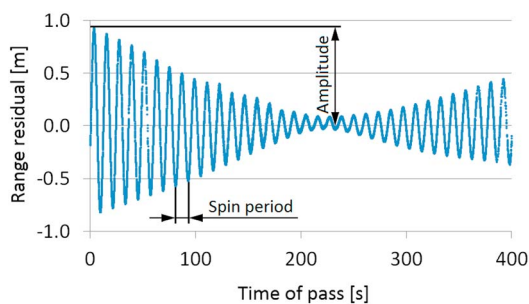


Figure 2. Example T/P SLR pass: Range residuals (observed minus calculated range) measured by Graz SLR station on 18 June 2014. The period and the amplitude of the oscillations are indicated. The 0 level represent the reference orbit.

2. Spin Parameters Determination

2.1. Satellite Orientation

The inertial orientation of the passive T/P makes the RRA visible from Earth and allows for laser ranging measurements to the spacecraft to be collected. An example of a T/P pass measured by the Graz high repetition rate SLR system is presented in Figure 2. The range residuals are computed as the difference between the measured and calculated ranges to the satellite—the zero level

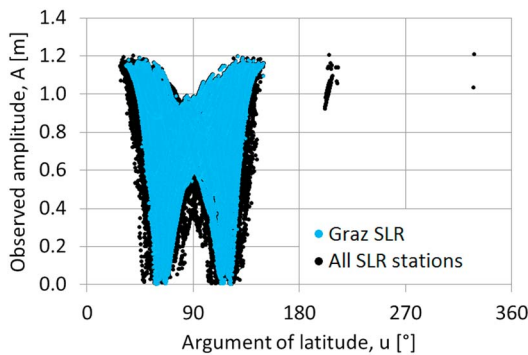


Figure 3. The amplitudes of the range residual oscillations measured by the SLR systems; 58,500 values measured from 10 June 2014 to 1 July 2016.

indicates the reference orbit. The range residuals oscillate with a stable period during the pass due to the rotation of the RRA about the spin axis of the satellite (Kucharski et al., 2014); the amplitude of the oscillation depends on the incident angle between the satellite station direction and the orientation of the spin axis.

The SLR passes measured from 10 June 2014 to 19 October 2016 provide 58,460 amplitude values (Figure 3) of which 39% were delivered by the Graz SLR (Station ID 7839, Austria), 24% by Changchun SLR (7237, China), and the remaining 37% by the stations: Potsdam SLR (7841, Germany), Herstmonceux (7840, United Kingdom), Matera (7941, Italy), San Fernando (7824, Spain), Riga (1884, Latvia), Sejong (7394, Korea), Mount Stromlo (7825, Australia), and Borowiec (7811, Poland).

Due to the stable orientation of the spacecraft with respect to the orbital plane, the visibility of the RRA from Earth surface is not uniform and limited from the Southern Hemisphere: there are only 10 passes of T/P measured by Mount Stromlo station (latitude of 35.316°S, amplitude data above $u = 180^\circ$) that were obtained below 60° of satellite elevation above the local horizon.

Assuming that the spin axis and the central axis of the RRA ring are parallel allows the amplitude of the range residual oscillation to be defined as $A = D \cdot \sin(\alpha)$, where D is an offset between the axes and α is an incident angle between the spin axis and the station vector (vector from the satellite center to the observing ground station) (Kucharski et al., 2014). The amplitude values are used to determine the orientation of the spacecraft: the minima occur when the station vector and the spin axis nearly coincide (the nadir panel of the spacecraft points toward the ground SLR system), while the maxima are measured when the station vector is perpendicular to the spin axis. The symmetrical distribution of the amplitudes with respect to the orbital plane suggests that the orientation of the satellite is stable within the orbital coordinate system (OCS)—which is defined as a right-handed Cartesian system with +X axis oriented as perigee and +Z being the normal vector to the orbital plane.

The known position of the satellite and the SLR ground station in the J2000 inertial reference frame, along with the observed amplitude A at a given epoch, allows for the calculation of the angle α between the spin axis and the station vector if the distance D is specified. The cone defined by the station vector as the central axis and the half-aperture angle α gives the circle of the possible spin axis orientations in the reference coordinate system. In order to determine the spin axis orientation, the amplitudes A_i measured within a 3 day span are collected and the corresponding angles α_i are calculated. It is assumed that the satellite orientation in the orbital coordinate system OCS remains stable over the 3 day period. The least squares method is used to determine the crossing point of the orientation circles that indicates the satellite spin axis coordinates. The average distance between obtained spin axis vector and the orientation circles gives the accuracy of the spin axis determination and depends on the assumed value of the offset D . The analysis is performed for D values in the range 1,100 mm to 1,300 mm, with the best accuracy of the spin axis determination of 1.7° achieved for $D = 1,130$ mm (± 5 mm).

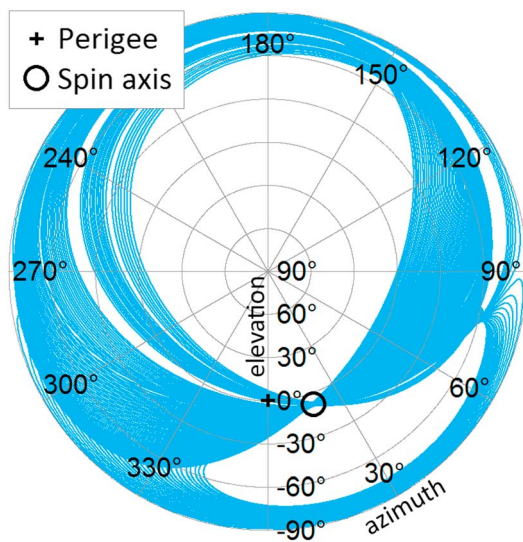


Figure 4. The orientation circles in the orbital coordinate system calculated for 132 amplitudes A measured during the 3 day period (26–29 October 2015). The intersection of the circles indicates the satellite spin axis orientation (azimuth = 18.7°, elevation = -7.8°); the position of the orbital perigee is at azimuth = 0°, elevation = 0°.

Figure 4 presents an example of the spin axis determination: 132 amplitudes A measured during 26–29 October 2015 define the orientation cones in the orbital coordinate system and the crossing point of the circles indicates the spin axis coordinates. The 401 spin axis orientation values determined (Figure 5) indicate nutation of the T/P spin axis in the vicinity of the orbital perigee vector (in the clockwise direction). A frequency analysis of the spin axis coordinates gives the nutation period of 101.3 days in azimuth and 101.8 days in elevation angle of the orbital coordinate system.

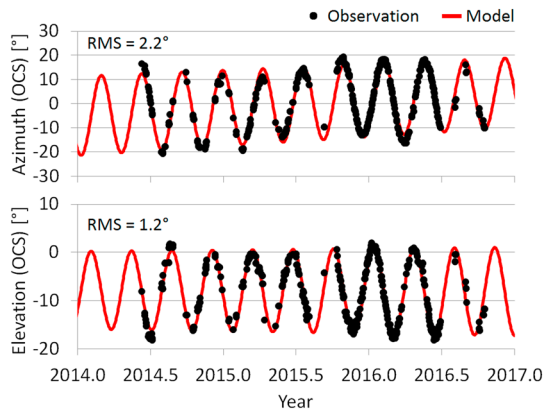


Figure 5. T/P spin axis orientation in orbital coordinate system. The coordinates of the orbital perigee are azimuth = 0° and elevation = 0°.

The determined spin axis coordinates in the orbital coordinate system S_{OCS} can be approximated by nonlinear functions:

$$\text{Azimuth} = -3.851 + 8.8506 \cdot 10^{-3} \text{ Day} + (-16.18 + 1.871 \cdot 10^{-3} \text{ Day}) \cdot \cos(1.972 + 62.11 \cdot 10^{-3} \text{ Day}) [^\circ], \text{ RMS} = 2.2^\circ,$$

$$\text{Elevation} = -7.867 - 0.2478 \cdot 10^{-3} \text{ Day} + (8.1671 + 1.008 \cdot 10^{-3} \text{ Day}) \cdot \cos(0.4233 + 62.11 \cdot 10^{-3} \text{ Day}) [^\circ], \text{ RMS} = 1.2^\circ,$$

where Day = MJD - 56,800.

The orientation of OCS is defined by the orbital plane and thus the inertial coordinates of the spin axis vector precess with the period of the orbital ascending node = 173.3 days. The celestial coordinates of the spin axis vector S_{CCS} can be calculated as

$$S_{CCS} = R_3(-\Omega)R_1(-i)R_3(-\omega)S_{OCS},$$

where R_1 and R_3 are the geodetic rotation matrices about the x axis and z axis, respectively, in a right-handed Cartesian coordinate system (Seeber, 2003), with the satellite orbital element parameters: Ω = right ascension of the ascending node, i = inclination, ω = argument of perigee. During the time span investigated (June 2014 to October 2016) the orbital argument of perigee remains between 267° and 275° with an average value of 270°.

2.2. Satellite Spin Period and Spin Direction

Photometric and SLR data were analyzed in order to determine the spin period of T/P. The light curves collected by the Odessa observatory provide the satellite brightness that changes significantly over a single pass due to the spin of the sunlit satellite (Koshkin, 2016). The light curves were processed with the phase dispersion minimization method, PDM (Stellingwerf, 1978), which finds the periodic variation in the time series by minimizing the dispersion of the folded data set. Unlike frequency analysis, PDM allows for the determination of long spin periods in relation to the pass duration. Figure 6 presents a phase-folded light curve (observed by Odessa on 13 May 2008) with the determined spin period of 28.6 s. In the case of the SLR data, the spin period is determined by using a frequency analysis of the range residual oscillations (Figure 2). The analysis employs the Lomb-Scargle algorithm (Kucharski et al., 2013; Lomb, 1976), which estimates a frequency spectrum of unequally spaced data, based on the least squares fit of sinusoids to the data samples.

The 1,281 photometric and SLR passes collected for T/P were processed, and the apparent spin period of the satellite as observed from the ground location was calculated. Since the position and orientation of the satellite (Figure 5), ground station, and the Sun are known, the apparent effect can be quantified and removed from the observations resulting in the inertial spin of the spacecraft. The apparent angle for the SLR systems depends on the azimuthal motion of the station vector about the satellite's spin axis (Kucharski et al., 2013) and varies on average in the range of $\pm 75^\circ$ for the passes analyzed. In the case of the photometry data, the apparent angle is a product of the azimuthal motion of two vectors pointing from the satellite toward the ground station and the Sun; the average range of the apparent angle for Odessa's location is $\pm 25^\circ$.

The observed apparent spin period can be corrected by the positive or negative apparent angle depending on the spin direction of the satellite. Figure 7a presents the apparent spin periods (SLR data) observed from several different geographical locations with the precision of the residuals calculated as 91.2 ms from the polynomial trend function; the precision is defined as a root-mean-square (RMS) of data spread. Applying the apparent correction with the assumption of a counterclockwise (CCW) spin direction improves the precision to 33.8 ms (the value of 169.2 ms is obtained for a clockwise spin direction). The improvement in the precision (Figure 7b) indicates a CCW inertial spin direction of T/P.

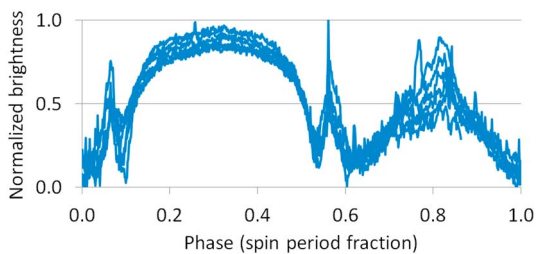


Figure 6. Example of a phase-folded light curve of T/P measured on 13 May 2008. The duration of the pass is 2 min:45 s, and the spin period determined with PDM is 28.6 s.

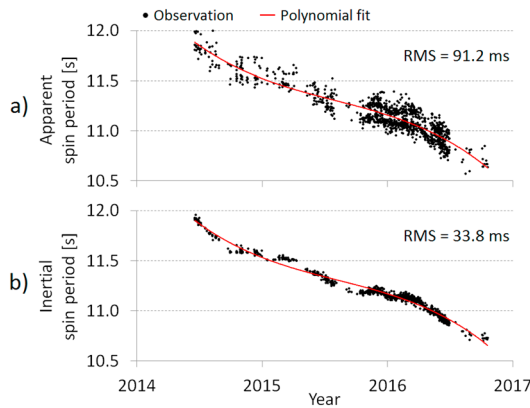


Figure 7. Spin direction determination. (a) The observed (apparent) spin period. (b) The measured values corrected for the apparent effect assuming a counter-clockwise spin direction of the satellite.

interacting with the surface elements of the spacecraft. The photons carry an amount of momentum given by their energy divided by the velocity of light, and this momentum can be exchanged during the interaction with a solid surface. The elementary force vector $d\vec{F}$ caused on a surface element dS of the spacecraft by the incident photon flux Φ is given by Milani et al. (1987)

$$d\vec{F} = -\frac{\Phi}{c} \left[(1 - \rho)\hat{R} + 2\left(\frac{\delta}{3} + \rho \cos\beta\right)\hat{n} \right] dS |\cos\beta|,$$

where c is the speed of light, ρ and δ represent the fraction of the incident light, which is reflected and diffused, respectively; the surface normal vector \hat{n} creates angle β with the direction vector toward the radiation source \hat{R} .

The dimensions, mass, and the optical properties of T/P are provided by the technical specification and define a satellite macromodel for the simulation of the dynamics. The orientation of the solar panel with respect to the body at the end of the mission was not specified by the operators and is investigated in this section.

The three photon fluxes considered in the spin simulations are as follows: the direct solar radiation Φ_{sun} , the Earth-reflected sunlight (albedo) Φ_{albedo} , and the Earth infrared emission Φ_{IR} . The direct solar flux is calculated as

$$\Phi_{\text{sun}} = \psi S \left(\frac{a_u}{r_0}\right)^2$$

with the solar radiation constant $S = 1,361 \text{ W/m}^2$ and scaled (0.1) by the realistic Earth shadow function ψ (Hubaux et al., 2012); a_u is the astronomical unit, and r_0 is the Sun-satellite distance.

The Earth fluxes are computed from the Clouds and the Earth's Radiant Energy System, CERES (Wielicki et al., 1996), an ongoing NASA climatological experiment from Earth orbit that measures the solar-reflected and Earth-emitted radiation from the top of the atmosphere to the Earth's surface. The model provides monthly values of the Earth albedo reflectivity and infrared emissivity as a function of geographical coordinates. The resulting photon flux directed toward a satellite is an integral over the Earth surface elements visible from the satellite position multiplied by the magnitude of the solar irradiation:

$$\Phi_{\text{albedo}} = S \left(\frac{a_u}{r_e}\right)^2 \sum_{\phi, \lambda} \left(\alpha_{\text{albedo}, \phi, \lambda} \cos\varphi_{\text{sun}} \cos\varphi_{\text{sat}} \frac{A_{\phi, \lambda}}{\pi d^2} \right),$$

$$\Phi_{\text{IR}} = S \left(\frac{a_u}{r_e}\right)^2 \sum_{\phi, \lambda} \left(\alpha_{\text{IR}, \phi, \lambda} \cos\varphi_{\text{sat}} \frac{A_{\phi, \lambda}}{4\pi d^2} \right),$$

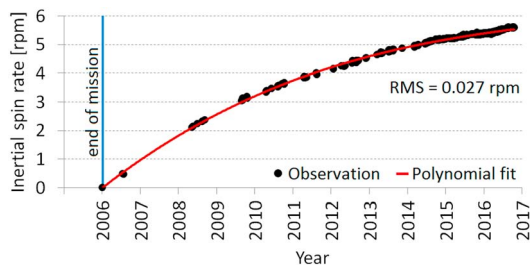


Figure 8. The history of T/P inertial spin rate: SLR and photometric data combined.

All of the inertial spin rates obtained are presented in Figure 8, which indicates a continuous increase in the rotational energy of the satellite over the 11 year time span. The trend can be approximated by the polynomial function:

$$\begin{aligned} \text{Rate} &= 3.2671 \cdot 10^{-11} \text{Day}^3 - 4.9917 \cdot 10^{-7} \text{Day}^2 + 2.8875 \cdot 10^{-3} \text{Day} \\ &\quad - 0.11257 \text{ [rpm]}, \text{ RMS} \\ &= 0.027 \text{ rpm}, \end{aligned}$$

where $\text{Day} = \text{MJD} - 53,700$.

3. Photon Radiation Pressure Effect on TOPEX/Poseidon

3.1. Photon Pressure Simulation

The spin energy of T/P has continuously increased since the end of the mission—from stable nadir pointing to the present, fast spinning state. The spin-up of T/P is caused by the solar radiation pressure

Table 1
TOPEX/Poseidon Macromodel Specification

Surface area [m ²]	Normal vector in satellite reference frame			Optical coefficients						
				Visible spectrum			Infrared spectrum			
	X	Y	Z	ρ	δ	α	ρ	δ	α	
4.71	1	0	0	0.201	0.375	0.424	0.081	0.150	0.769	
4.71	-1	0	0	0.244	0.386	0.370	0.002	0.003	0.995	
8.18	0	1	0	0.886	0.302	-0.188	0.095	0.032	0.873	
8.18	0	-1	0	0.782	0.339	-0.121	0.200	0.086	0.714	
8.32	0	0	1	0.239	0.390	0.371	0.087	0.143	0.770	
8.32	0	0	-1	0.275	0.363	0.362	0.109	0.145	0.746	
Solar array										
25.5	Front (originally to Sun)			0.050	0.220	0.730	0.024	0.106	0.870	
25.5	Back			0.170	0.660	0.170	0.025	0.095	0.880	

Note. The optical coefficients indicate ρ = specular reflection, δ = diffusion, α = absorption of the surfaces.

where r_e is the Sun-Earth distance, d is the Earth-satellite distance, ϕ and λ are the latitude and longitude coordinates of the Earth surface element of area $A_{\phi, \lambda}$. The parameters $\alpha_{\text{albedo}, \phi, \lambda}$ and $\alpha_{\text{IR}, \phi, \lambda}$ are the CERES reflectivity and emissivity coefficients, φ_{sun} and φ_{sat} represent the incident angles between the normal to the Earth surface element and the direction to the Sun and satellite, respectively.

The satellite position is provided by the Austrian Academy of Sciences prediction center (Wirnsberger et al., 2015) in the Consolidated Prediction Format, and the inertial orientation of the spacecraft is given by the equations from section II-A. The simulations are performed with the fourth-order Runge-Kutta method and cover the time span from June 2014 to October 2016 during which the highly accurate laser ranging data allowed for the satellite orientation to be determined.

During a single simulation step at a given epoch time, the satellite inertial position, orientation, and the incident flux vectors are determined. The photon pressure forces and torques are calculated for all elementary surface elements of the satellite macromodel (Table 1) and integrated. The spin period trends are simulated for the full range of the solar panel pitch angles (with a 1° step) and summary results are presented in Figure 9.

The best fit between the predicted and observed spin period trends occurs for a solar panel pitch angle of 105° with the precision of the spin period residual (observed minus calculated) of 21 ms. The simulations indicate that the spin dynamics of T/P strongly depend on the geometry of the satellite platform defined by the pitch angle of the solar panel. The rate of spin period change has an average value of -1.46 ms/d (Figure 9b) and depends on the satellite surface area exposed to the solar photon flux, which varies from 8.2 m² to 34 m² (average 25.1 m²) with a frequency of the spin rate. The most intense spin-up of T/P occurs for an incident angle larger than 90° between the satellite-Sun direction and the spin axis vector (Figure 9c).

3.2. Photon Pressure Force and Torque

The incident photon fluxes exert force on the exposed surface area of the satellite and perturb its orbital motion. Figure 10a presents the along-track projection of the force vectors produced on the satellite by the combination of the photon fluxes versus elongation angle (Earth centered angle between directions to the Sun and satellite).

The combined photon pressure force in the along-track direction of the satellite orbital motion oscillates due to the spin of the body and is asymmetrically distributed over the range of ±220 μN. The force component caused by the direct solar radiation pressure reduces to zero

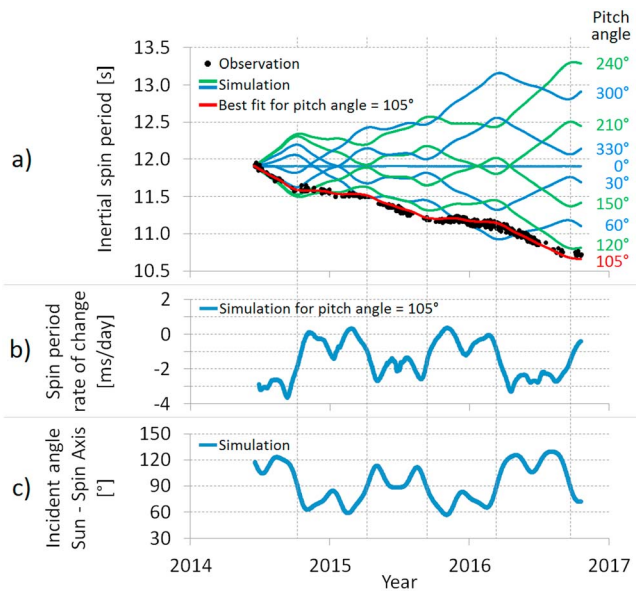


Figure 9. Determination of the solar panel orientation. (a) The observed (SLR) and simulated spin trends for selected pitch angles of the solar panel. (b) The rate of change of the simulated spin period for solar panel pitch angle of 105°. (c) The incident angle between the satellite-Sun direction and the spin axis vector (the vertical lines indicate an incident angle of 90°).

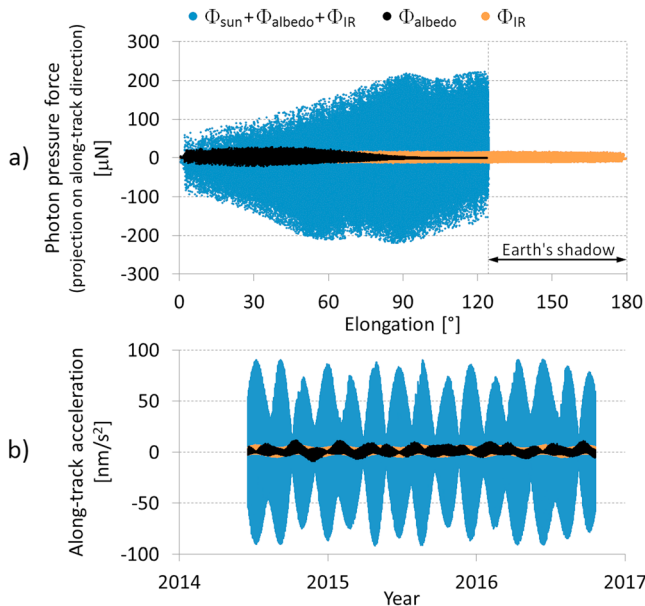


Figure 10. Simulated along-track effects. (a) Along-track projection of the force vectors caused by the incident photon fluxes. T/P is in the Earth's shadow for elongation angles above 124.4°. (b) Along-track acceleration on T/P caused by the photon fluxes versus time.

presents 1 day average of the torque component. By contrast, the average value in the Earth's albedo case is 3.1 μNm and at -0.1 μNm for the Earth IR radiation. Figure 11c gives a simulated trend of T/P spin energy $E_{\text{spin}} = 0.5I\omega^2$, where I is the satellite moment of inertia (estimated to be 70,000 kg m²) and ω is the spin rate of the body in rad/s; the vertical lines indicate time spans of slowly and rapidly increasing spin energy. The rapid spin-up of the satellite occurs when the incident angle between the photon force vector and the spin axis is lower than 90°.

when the satellite enters the Earth's shadow at an elongation angle of 124.4°. The force component caused by the Earth's albedo does not exceed ±29 μN and decreases to 0 μN for elongation angles above 90°. The Earth infrared emission component oscillates within a stable band of ±17 μN throughout the full elongation range. The force in the along-track direction is particularly useful for the analysis of the accelerations perturbing the orbital motion of the satellite and causing the orbit to decay. The magnitude of the along-track accelerations changes over time (Figure 10b) due to the precession of the orbital plane, which determines the inertial orientation of the spacecraft.

The direct solar radiation is the major photon flux interacting with the satellite and exerts force depending on the satellite cross-sectional area exposed to the Sun. The magnitude of the force changes between 65 μN and 228 μN and has a mean value of 138.6 μN (Figure 11a).

The force acting on the surface elements of the spacecraft generates torque defined as the cross product of the surface offset vector from the body center of mass and the force vector. The projection of the torque vector on the spin axis determines its impact on the spin rate: the spin-up occurs when the incident angle between the torque vector and the spin axis vector is lower than 90°. The instantaneous torque projection on the spin axis vector varies between -758 μNm and 984 μNm and has an average value of 71 μNm; Figure 11b presents

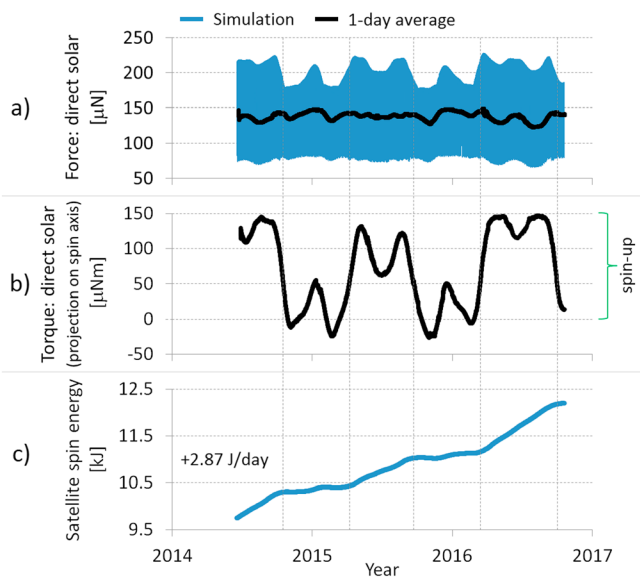


Figure 11. Simulated direct solar pressure effect. (a) Magnitude of the direct solar radiation force on T/P. (b) A 1 day average of the torque component in the spin axis direction. (c) Satellite spin energy.

4. Discussion

The space debris objects orbiting the Earth are exposed to environmental forces with the dynamics perturbed by the Earth's gravity and magnetic fields, third-body effects, solar radiation pressure, atmospheric drag, or even electrostatic effects. The passive, optical observations of the T/P spin dynamics allow for the physical analysis of the photon radiation pressure effect on the box wing-type satellite.

The inertial orientation of the spin axis changes with a precession period of 173.3 days and a mean nutation period of 101.6 days remaining in the vicinity of the orbital perigee vector. The synchronization of the satellite's orientation with the orbital coordinate system OCS can be caused by the Earth's gravitational field acting on the dynamical oblateness (the difference in the principal moments of inertia) of the spacecraft as was observed with the geodetic satellite Ajisai (Kucharski et al., 2016).

The continuous spin-up of T/P is shown to be caused by the surface interaction with direct solar radiation flux. The gain in the satellite spin energy is not constant and depends on the value of the photon torque projection on the spin axis (Figure 11).

Satellite attitude modeling allows for a realistic estimation of the surface forces and perturbations (Figure 10b) which can improve the orbit prediction accuracy for conjunction analyses.

5. Conclusions

The long-term optical observations of T/P allow for the accurate determination of the spacecraft spin dynamics. The laser range measurements to the satellite's RRA give information on the T/P inertial spin axis orientation with the accuracy of 1.7° (Figure 5). The physical analysis of the observed spin dynamics makes it possible to find the orientation of the solar panel with respect to the spacecraft body and model the spin period trend with the precision of 21 ms.

The direct solar photon flux is identified to be the main environmental factor responsible for the increase of T/P spin energy at an average rate of 2.87 J/day. The complete attitude model allows for the surface force and drag estimation (Figure 10b) which is needed in the orbit determination process and improves accuracy of the space debris conjunction analyses.

Acknowledgments

We acknowledge the use of data provided by Graz SLR station and obtained within the ESA project "Debris Attitude Motion Measurements and Modelling" (Project 40000112447), as well as the other SLR systems organized within the International Laser Ranging Service. This research is supported by the Cooperative Research Centre for Space Environment Management, SERC Limited, through the Australian Government's Cooperative Research Centre Programme. The authors express their thanks to Remko Scharroo of the European Organisation for the Exploitation of Meteorological Satellites (EUMETSAT) for his expert advice on the TOPEX/Poseidon analysis. We thank the observers and technical staff operating the telescope systems for their devotion to obtain the high-quality measurements used in this project. The SLR data are freely available from the Graz FTP server (<ftp://sddis.oeaw.ac.at>) and located in directory `"/pub/fr_crd/topex,"` the CPF predictions: `"/pub/cpf_predicts/topex";` the measured spin trend data (Figures 7 and 8): `"/pub/sci_product/topex"`. The light curves are available through the Light Curve Atlas (Koshkin, 2016).

References

- Bennett, J. C., Sang, J., Smith, C. H., & Zhang, K. (2013). Accurate orbit predictions for debris orbit manoeuvre using ground-based lasers. *Advances in Space Research*, 52(11), 1876–1887. <https://doi.org/10.1016/j.asr.2013.08.029>
- Fu, L. L., Christensen, E. J., Yamarone, C. A. Jr., Lefebvre, M., Ménard, Y., Dorrer, M., & Escudier, P. (1994). TOPEX/Poseidon mission overview. *Journal of Geophysical Research*, 99(C12), 24,369–24,381. <https://doi.org/10.1029/94JC01761>
- Hubaux, C., Lemaitre, A., Delsate, N., & Carletti, T. (2012). Symplectic integration of space debris motion considering several Earth's shadowing models. *Advances in Space Research*, 49(10), 1472–1486. <https://doi.org/10.1016/j.asr.2012.02.009>
- Kirchner, G., Koidl, F., Friederich, F., Buske, I., Völker, U., & Riede, W. (2013). Laser measurements to space debris from Graz SLR station. *Advances in Space Research*, 51(1), 21–24. <https://doi.org/10.1016/j.asr.2012.08.009>
- Koshkin, N. (2016). The atlas of light curves of space objects. Retrieved from <http://dspace.onu.edu.ua:8080/handle/123456789/8480>
- Koshkin, N., Korobeynikova, E., Shakun, L., Strakhova, S., & Tang, Z. H. (2016). Remote sensing of the Envisat and Cbers-2B satellites rotation around the centre of mass by photometry. *Advances in Space Research*, 58(3), 358–371. <https://doi.org/10.1016/j.asr.2016.04.024>
- Kucharski, D., Kirchner, G., Koidl, F., Fan, C., Carman, R., Moore, C., ... Feng, Q. (2014). Attitude and spin period of space debris Envisat measured by Satellite Laser Ranging. *IEEE Transactions on Geoscience and Remote Sensing*, 52(12), 7651–7657. <https://doi.org/10.1109/TGRS.2014.2316138>
- Kucharski, D., Kirchner, G., Otsubo, T., Lim, H.-C., Bennett, J., Koidl, F., ... Hwang, J.-Y. (2016). Confirmation of gravitationally induced attitude drift of spinning satellite Ajisai with Graz high repetition rate SLR data. *Advances in Space Research*, 57(4), 983–990. <https://doi.org/10.1016/j.asr.2015.12.010>
- Kucharski, D., Lim, H.-C., Kirchner, G., & Hwang, J.-Y. (2013). Spin parameters of LAGEOS-1 and LAGEOS-2 spectrally determined from Satellite Laser Ranging data. *Advances in Space Research*, 52(7), 1332–1338. <https://doi.org/10.1016/j.asr.2013.07.007>
- Lomb, N. R. (1976). Least-squares frequency analysis of unequally spaced data. *Astrophysics and Space Science*, 39(2), 447–462. <https://doi.org/10.1007/BF00648343>
- Milani, A., Nobili, A. M., & Farinella, P. (1987). *Non-gravitational perturbations and satellite geodesy*. Bristol: Adam Hilger Ltd.
- Paredes, E., Navarro, A., Vincent, M., Ceva, J., & Salama, A. (2008). TOPEX/Poseidon End-of-Life Navigation Operations and Decommissioning Summary, SpaceOps 2008 Conference. Heidelberg, Germany. <https://doi.org/10.2514/6.2008-3443>
- Pearlman, M. R., Degnan, J. J., & Bosworth, J. M. (2002). The International Laser Ranging Service. *Advances in Space Research*, 30(2), 135–143. [https://doi.org/10.1016/S0273-1177\(02\)00277-6](https://doi.org/10.1016/S0273-1177(02)00277-6)
- Schwartz, J. A. (1990). Laser ranging error budget for the TOPEX/Poseidon satellite. *Applied Optics*, 29(25), 3590–3596. <https://doi.org/10.1364/AO.29.003590>
- Seeber, G. (2003). *Satellite geodesy* (2nd ed.). Berlin: Walter de Gruyter. <https://doi.org/10.1515/9783110200089>
- Shakun, L., Koshkin, N., Korobeynikova, E., Melikyants, S., Strakhova, S., Terpan, S., ... Ryabov, A. (2016). The observations of artificial satellites and space debris using KT-50 telescope in the Odessa University. *Odessa Astronomical Publications*, 29, 217–220. <https://doi.org/10.18524/1810-4215.2016.29.85234>
- Stellingwerf, R. F. (1978). Period determination using phase dispersion minimization. *Astrophysical Journal*, 224(Part 1), 953–960. <https://doi.org/10.1086/156444>
- Tapley, B. D., Ries, J. C., Davis, G. W., Eanes, R. J., Schutz, B. E., Shum, C. K., ... Zelensky, N. P. (1994). Precision orbit determination for TOPEX/Poseidon. *Journal of Geophysical Research*, 99(C12), 24,383–24,404. <https://doi.org/10.1029/94JC01645>
- Wielicki, B. A., Barkstrom, B. R., Harrison, E. F., Lee, R. B. III, Louis Smith, G., & Cooper, J. E. (1996). Clouds and the Earth's radiant energy system (CERES): An Earth observing system experiment. *Bulletin of the American Meteorological Society*, 77(5), 853–868. [https://doi.org/10.1175/1520-0477\(1996\)077%3C0853:CATERE%3E2.0.CO;2](https://doi.org/10.1175/1520-0477(1996)077%3C0853:CATERE%3E2.0.CO;2)
- Wirnsberger, H., Baur, O., & Kirchner, G. (2015). Space debris orbit prediction errors using bi-static laser observations. Case study: ENVISAT. *Advances in Space Research*, 55(11), 2607–2615. <https://doi.org/10.1016/j.asr.2015.02.018>